CrossMark

RESEARCH ARTICLE

Low-cost magnetic herbal biochar: characterization and application for antibiotic removal

Xiangrui Kong[1] · Yaoxuan Liu[1] · Jiachang Pi[1] · Wenhong Li[1] · QianJiahua Liao[1] ·
Jingge Shang[1,2] (iD)

Abstract Magnetic biochar (M-BC) was derived from herbal medicine waste, *Astragalus membranaceus* residue, and was used as an adsorbent for ciprofloxacin removal from aqueous solutions. The M-BC was characterized by Brunauer–Emmett–Teller surface area analyses, Fourier transform infrared spectrometry, X-ray diffraction analysis, hysteresis loops, scanning electron microscopy energy-dispersive spectrometry, and X-ray photoelectron spectroscopy. The BET surface area increased from 4.40 to 203.70 m^2/g after pyrolysis/magnetic modification. Batch experiments were performed at different dosages, initial concentrations, contact times, and solution pHs. Adsorption performances were evaluated using Langmuir and Freundlich isotherm models, and the results indicated that the Langmuir model appropriately described the adsorption process. The kinetic data were better fitted by a pseudo-second-order kinetic model. The maximum ciprofloxacin removal was observed at pH 6 (adsorption capacity of 68.9 ± 3.23 mg/g). Studies demonstrated that magnetically modified biochar might be an attractive, cost-effective, and easily separated adsorbent for contaminated water.

Xiangrui Kong and Yaoxuan Liu contributed equally to this work

Responsible editor: Hailong Wang

✉ Jingge Shang
  shangjingge@gmail.com; gege@cpu.edu.cn

[1] Department of Environmental Science, China Pharmaceutical University, Nanjing 210009, China

[2] State Key Laboratory of Lake Science and Environment, Nanjing Institute of Geography and Limnology, Chinese Academy of Sciences, Nanjing 210008, China

Introduction

Antibiotics, which have been widely used in veterinary and human medicine in recent decades, have become a serious threat to the environment and public health. The consumption of antibiotics has gradually increased because of rapid global economic and population growth. An estimated 162,000 tons of antibiotics was used in China in 2013 (Zhang et al. 2015), which could have dangerous effects on non-target organisms because of their intrinsic bioactivity and bioavailability. A very clear example is the increased antibiotic resistance genes (ARGs) in environment. The bacterial antibiotic resistance may be intrinsic or acquired through spontaneous mutations, but the cumulative effect is responsible for this phenomenon (Sharma et al. 2016). Additionally, many antibiotics cannot be completely absorbed and metabolized; the majority is excreted unchanged in feces and urine and then discharged directly into an aquatic environment and indirectly as domestic and industrial waste effluents, animal manure, and municipal wastewater treatments (Zhang et al. 2015). However, their parent compounds and metabolites are potentially toxic to humans through the food chain and drinking water (García-Galán et al. 2011). From a biological perspective, the evolution of the microbial structure can be influenced by antibiotics and may thus break the ecological balance (Berendonk et al. 2015). Many investigations have been conducted to control the threats of antibiotics to human health and the environment using such methods as chemical oxidation (Ji et al. 2015), sorption (Martins et al. 2015), and membrane separation(Cheng et al. 2016). The use of a high-capacity adsorbent to remove various contaminants in the aqueous phase is considered to be the best method. Examples include adsorption of bacteriocins from clay

nanoparticles (Meira et al. 2015) and removing ciprofloxacin with carbon nanotubes and activated carbon (Li et al. 2014).

Biochar is biomass with a stable porous structure that is heated by a carbon-rich solid in limited oxygen or anaerobic conditions and is typically considered to be a highly efficient, cost-effective, and environmentally friendly adsorbent (Ahmad et al. 2014; Inyang &Dickenson 2015). Example applications of biochar include the adsorption of heavy metals, such as Fe, Mn, Cu, Cr, Pb, and Zn; preparations from *Concarpus*, wood, straw, or dairy manure biochar(Al-Wabel et al. 2015; Tytłak et al. 2015; Wu et al. 2016; Xu et al. 2013); removal of nitrogen with palm biochar from leaf sheaths(Li et al. 2016); removal of methylene blue by pine wood, pig manure, and cardboard biochar(Lonappan et al. 2016); adsorption of aromatic compounds with biochar prepared from bamboo (Yang et al. 2016); and removal of sulfamethoxazole with biomass biochar(Lian et al. 2014).

However, it is difficult to separate the biochar powder from solution. Previous studies proved that modifying the adsorbent with magnetic nanoparticles would be a useful method to separate small particle powders in solution with external magnetic fields; this method has a higher efficiency than the traditional centrifugation or filtration method, particularly in high suspended solids or oil-contaminated water. Ambashta et al. (2010) reviewed the magnetic materials used for water pollution control. Many magnetic adsorbents have been used to remove pollutants from water, including magnetite zeolites to remove heavy metals; magnetite activated carbon to remove Pb^{2+} and tetrabromobisphenol in the aqueous phase; magnetic graphene oxide for the removal arsenic; and magnetic biochar to remove cadmium, lead, and arsenic (Zhang et al. 2013; Mohan et al. 2014; Zhou et al. 2014a; Zhou et al. 2014b; Nodeh et al. 2016). In addition, magnetic adsorbents can be easily separated by a simple magnetic method from high suspended solids or oil-contaminated water.

Several million tons of herb residues are produced every year in China. Converting herb residues into biochar is a "win–win" solution for both Chinese herbal medicine manufacturing and environmental protection. In the present research, magnetic biochar (M-BC) derived from *Astragalus membranaceus* residues was used to adsorb ciprofloxacin (CIP). The main objectives of this study are to (1) prepare M-BC to improve the capacity of adsorption and (2) investigate the adsorption ability of M-BC for ciprofloxacin removal. The magnetic hysteresis curve, BET surface area (S_{BET}), Fourier transform spectroscopy (FTIR), X-ray diffraction analysis (XRD), and scanning electron microscopy energy-dispersive spectrometry (SEM-EDS) were also used to characterize the structure of the M-BC.

Materials and methods

### Preparation and characterization of M-BC

A. membranaceus residue, a traditional Chinese herbal medicine, was ground with a 100-mesh sieve and then subjected to thermal activation at 700 °C for 3 h under oxygen-limited conditions. After pyrolysis activation, the residues were treated with 1 mol/L HCl to remove the suspended ash. M-BC was prepared using the method described by Wang et al. (2014). Ferric and ferrous mixed solutions were prepared from 20 g of $FeCl_3·6H_2O$ and 11.1 g of $FeSO_4·7H_2O$ with 600 mL of deionized (DI) water. Then, the Fe^{3+}/Fe^{2+} mixed solution was dropped into the biochar suspension (20 g of biochar with 200 mL of DI water) and stirred vigorously under 25 °C for 60 min in a N_2 atmosphere. The pH of the mixed biochar/Fe^{3+}/Fe^{2+} suspension was adjusted to 10.5 with NaOH solution (10 mol/L). After being stirred for 60 min, the suspension was boiled under a N_2 atmosphere for 1 h and aged overnight at room temperature; then, the suspension was filtered and rinsed with DI water and ethanol several times and dried at 70–80 °C.

The specific surface area (S_{BET}) was evaluated from the N_2 adsorption isotherms with an ASAP2020 surface area and porosity analyzer (Micromeritics, Norcross, GA, USA). The surface morphologies and EDS data were examined using JEOL-7800 scanning electron microscopy (JEOL Ltd., Tokyo, Japan) and energy-dispersive spectroscopy (EDS) analysis with an Oxford INCA EDS detector. The X-ray diffraction (XRD) measurements were recorded on a Shimadzu XRD F-7000 using Cu-$K\alpha$(k = 1.54 Å) radiation at 40 kV and 30 mA; samples were scanned from 5 to 90 °C with a step size of 0.02°. The magnetic properties of M-BC were assessed using a vibrating sample magnetometer (SQUID-VSM, Quantum Design, USA).

Sorption experiments

Batch sorption experiments were carried out to study the behaviors of ciprofloxacin on the M-BC. The effects of different adsorbent doses, solution pH levels, sorption thermodynamics, and sorption kinetics were discussed. The influence of M-BC doses (1–20 g/L) was studied at room temperature and a CIP concentration of 200 mg/L. All of the centrifuge tubes were kept in the dark and shaken for 12 h to reach apparent sorption equilibrium according to the preliminary experiment. In the study of the effects of sorption kinetics, 0.05 g of M-BC and 25 mL of CIP (55, 110, and 220 mg/L) solution was added into 50 mL of Nalgene Oak Ridge centrifuge tubes at room temperature (25 °C). All of the centrifuge tubes were then kept in the dark and shaken at 160 rpm. The

Fig. 1 SEM and EDS spectra of magnetic biochar (M-BC)
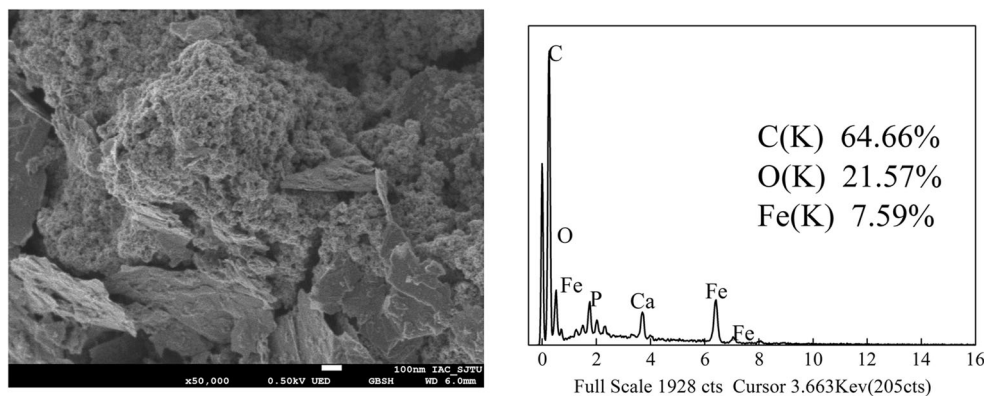
samples were separately shaken for 0 min, 10 min, 30 min, 1 h, 2 h, 3 h, 4 h, 6 h, and 12 h. In the sorption isotherm experiments, the initial CIP concentrations were set in the range of 5–300 mg/L. In the experiment on the effect of pH on CIP sorption, the pH of the initial solution was adjusted from 3.0 to 10.0 using HCl or NaOH solution, and 0.05 g of M-BC was added to 50 mL Nalgene Oak Ridge centrifuge tubes containing 25 mL of different pH levels of CIP solutions. Each treatment had three replications. After adsorption, the solution was filtered with a 0.22-μm filter membrane. The CIP concentrations were analyzed directly by an Agilent 1260 Infinity HPLC system (Agilent, USA) with a reversed-phase C18 column (250 mm × 4.60 mm, I.D., 5 μm, Agilent Technologies) at 270 nm. The mobile phase was 75/25 citric acid (0.05 mol/L)/acetonitrile, and the pH of the mixed

solution was adjusted to 3.5 using triethylamine. The flow rate was 1.0 mL/min, and the injection volume was 10 μL.

Results and discussion

Biochar characterization

The S_{BET} ranged from 4.40 m²/g (natural residue) to 203.70 m²/g (MBC). This significant increase in S_{BET} could be attributed to the pyrolysis processes. The surface area characteristics of the M-BC are shown in SEM-EDS (Fig. 1). XRD analyses (Fig. 2) were carried out to further investigate the MBC characteristics. The surface of the M-BC was covered by iron oxide, as suggested by the morphology of the

Fig. 2 Power XRD of magnetic biochar (M-BC)
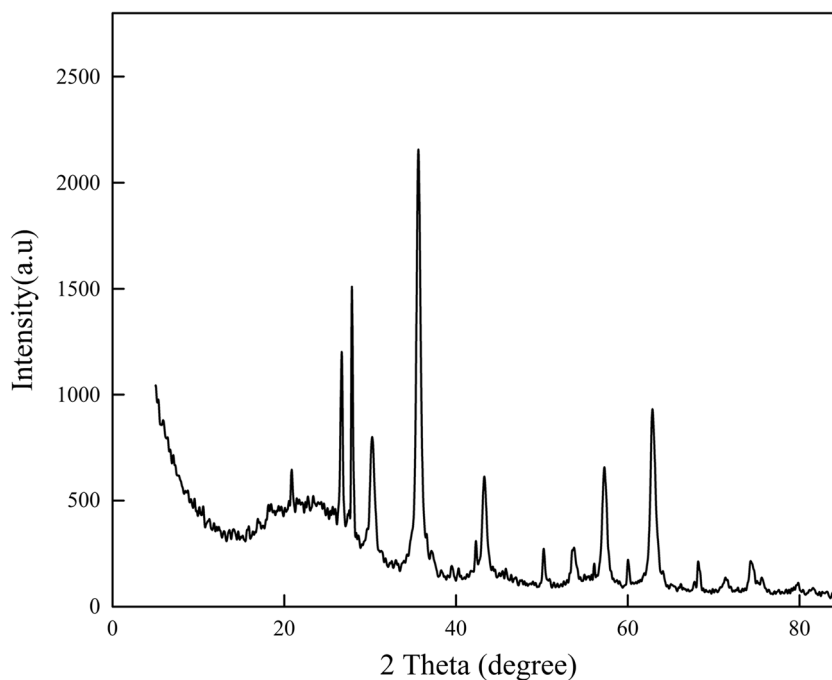
Fig. 3 Magnetic hysteresis loop
of M-BC
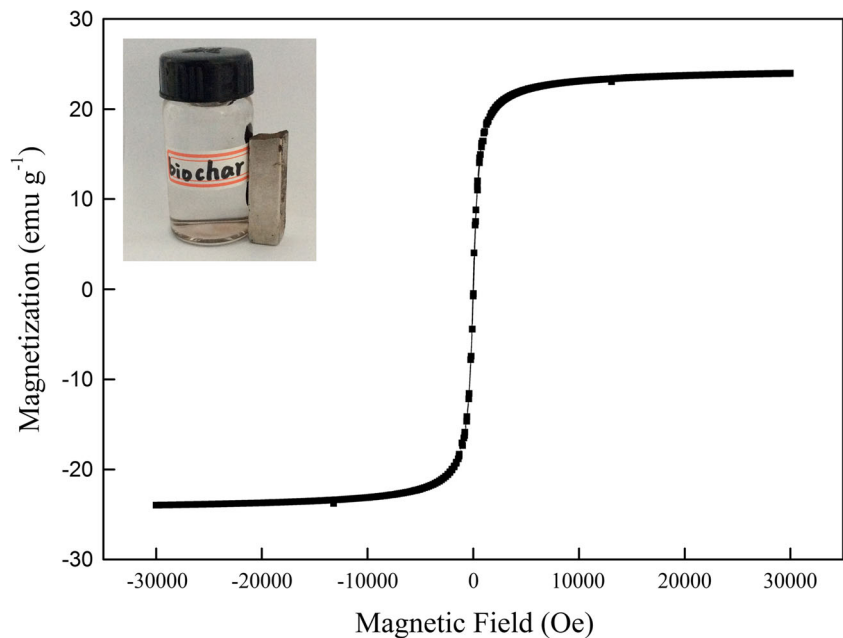
composite. According to the analysis of the element composition of the composite, the M-BC mainly contained carbon, oxygen, and iron. The content of iron was 7.59%, which is higher than that of the magnetic carbon composite prepared from waste hydrochar (3.39%) (Zhu et al. 2014). The differences in iron content may result from the different methods that were used to prepare magnetic composites and different biochar composition and structures. Furthermore, although some of the pores of M-BC are blocked by the presence of iron oxide particles, the composites still retain a large BET

surface area, which provided higher adsorption sites for the adsorbate (Ahmad et al. 2012).

The structure and phase composition of the M-BC are shown in the XRD patterns (Fig. 2). Multiple sharp iron oxide phase peaks were observed in the 2θ range of 5–90 °C. These peaks demonstrate the existence of crystallinity in phases present in the M-BCs. The peaks at 27.86, 30.24, 35.63, 43.3, and 57.27 are assigned to iron oxide and Fe_2O_3 (Maghemite-C/Q, PDF Number 01–025-1402, 00–039-1346) in M-BC. These peaks correspond to the five indexed

Fig. 4 FTIR spectra of M-BC
and herb residue
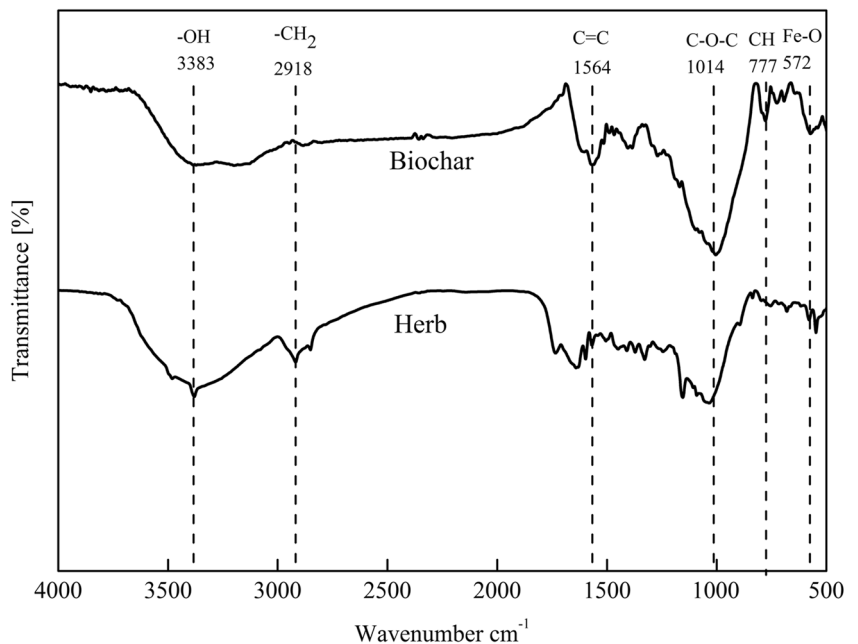
Fig. 5 Adsorption capacity and removal efficiency for CIP. (Experiment conditions: initial CIP concentration of 100 mg/L, temperature of 25 °C)
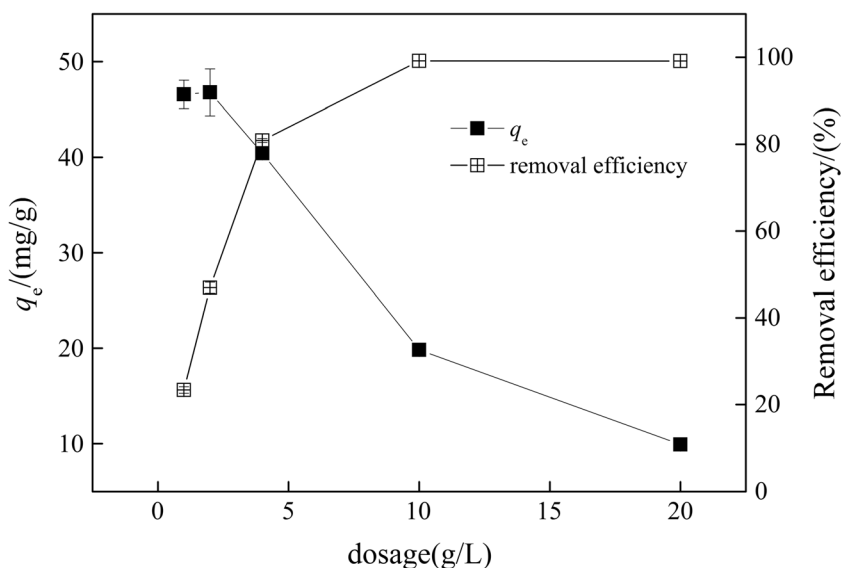

planes (205), (220), (311), (400), and (511) of Maghemite. The M-BC peaks at 43.3, 53.6(422), and 62.94 are assigned to Fe_3O_4 (PDF Number 01–088-0315). The results of the XRD analysis confirmed that M-BC was prepared.

The magnetic behaviors of the MBC were studied using the vibrating sample magnetometer (VSM) at 25 °C. The magnetic hysteresis curves for M-BC are shown in Fig. 3. The results demonstrated that the saturation magnetization value was 23.96 emu/g. This result is lower than those for the magnetic field of pure ferriferrous oxide (54.3–88.7 emu/g) (Fan et al. 2011) and the Fe_3O_4/HNTs@C nanohybrid (24.5 emu/g at 25 °C) (Tian et al. 2016) but higher than that for magnetic energy cane biochar (0.82 emu/g at 27 °C), as described by Mohan (Mohan et al. 2015). The difference among the saturation magnetization may result from the existence of biochar and the small size of the magnetic particles (Do et al. 2011).

The EDS results demonstrate that the iron content was 7.59% in M-BC. The EDS and magnetic hysteresis loop results demonstrated that M-BC could be attracted by magnets, which would be beneficial for pollutant separation and adsorbent recycled with magnets.

The FTIR spectra of the adsorbent before the adsorption experiments are shown in Fig. 4. The peak at approximately 572.4 cm^{-1} is assigned to Fe–O bands(Lim et al. 2009); the broad band at 3383 cm^{-1} is assigned to the stretching vibration of the hydroxyl groups (–OH) and the peak at 777 cm^{-1} is ascribed to aromatic C–H. The bands at 2918 and 1564 cm^{-1} correspond to CH_2 and C = O, respectively. The peak at 1014 cm^{-1} is assigned to aromatic C–O–C stretching vibration. These relative peaks indicate that massive original organic residues, including polymeric CH_2, lignin and fatty acids, are present on the surface of M-BC.
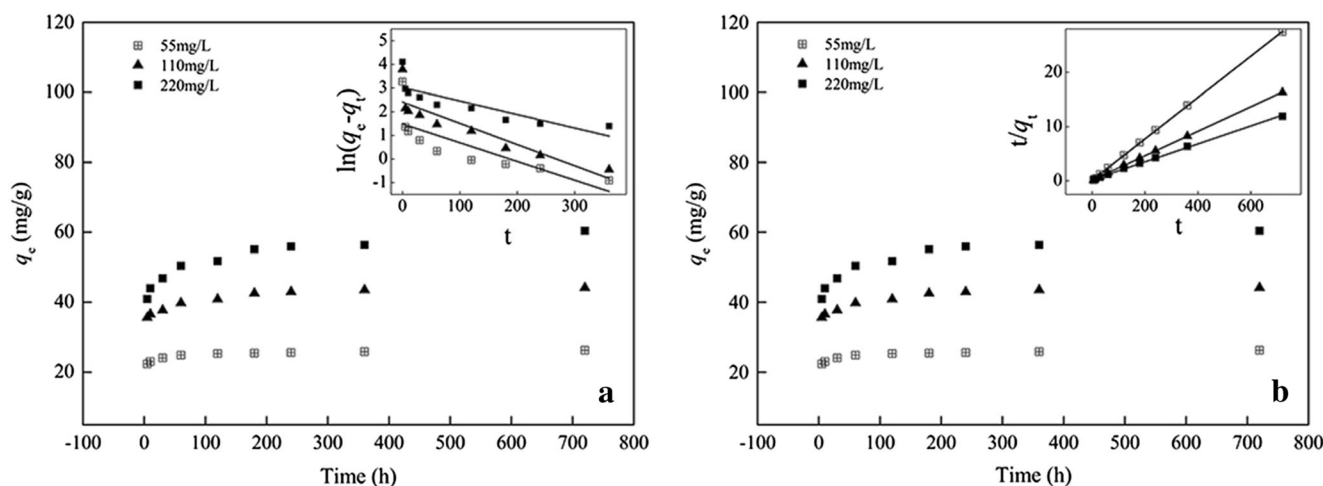
Fig. 6 Pseudo-first-order (**a**) and second-order (**b**) kinetic models for CIP adsorption by M-BC at different initial concentrations

Table 1 Surface area characteristics of M-BC and natural *Astragalus mongholicus* residue

Surface area characteristics of MBC and herb residue[a]	
S_{BET} (m^2/g)	203.70 (4.40)
Smic (m^2/g)[b]	89.34 (ND[c])
V_T (cm^3/g)[d]	0.187 (0.023)
Vmic (cm^3/g)[e]	0.041 (ND)

[a] Values in the parentheses are for natural *Astragalus mongholicus* residue

[b] Micropore surface area calculated using the t-plot method

[c] ND: The value was not sufficiently large to measure

[d] Total pore volume

[e] Micropore volume calculated with the t-plot method

Effect of adsorbent dosage

The removal efficiency and adsorption capacity of ciprofloxacin onto M-BC with an initial concentration of 200 mgL^{-1} are shown in Fig. 5. The adsorption capacity of CIP(q_e) decreased with increasing M-BC dosage, whereas the removal efficiency increased from 23.4 to 99.1%. Similar behavior was reported with biochar prepared from anaerobic digestion residue, palm bark, and eucalyptus for the adsorption of methylene blue dye (Sun et al. 2013), and the increase in removal efficiency is likely the result of the increased size of the available sorption surface(Ahmad et al. 2014).

Adsorption kinetics

The sorption of CIP on M-BC exhibited two phases. The adsorption increased rapidly during the first 2 h and then increased more gradually until reaching sorption equilibria after approximately 12 h (Fig. 6). The M-BC exhibited a rapid adsorption of CIP, which was attributed to the greater sorption of the contaminant on the surface of the

adsorbent compared to in the micropores (Shan et al. 2016).

To predict the mechanism of the adsorption process of CIP onto M-BC, the pseudo-first-order (Eq. 1) and pseudo-second-order models (Eq. 2) were tested to fit the adsorption experimental data; the values of the rate constant (k_1), the regression coefficients (R^2) and the adsorption capacity are listed in Tables 1 and 2.

$$\log(q_e - q_t) = \log q_e - k_1 t \qquad (1)$$

$$\frac{t}{q_t} = \frac{1}{k_2 q_e^2} + \frac{t}{q_e} \qquad (2)$$

where q_e and q_t (mg/g) correspond to the amount of CIP adsorbed per gram of adsorbent at equilibrium and at time t, respectively. k_1 (min^{-1}) and k_2(g mg^{-1} min^{-1}) are the rate constants of the pseudo-first-order and pseudo-second-order adsorption, respectively.

The regression coefficients ($R^2 > 0.999$) for the pseudo-second-order models were higher than those for the pseudo-first-order models ($R^2 > 0.639$), as shown in Fig.6 and Table 2. These results indicate that the adsorption kinetics are better represented by the pseudo-second-order kinetic model.

The reactions involved in the pseudo-second-order model are greatly influenced by the amount of CIP on the M-BC surface and the amount of CIP adsorbed at equilibrium. This relationship means that the rate of the adsorption processes is directly proportional to the number of active sites on the M-BC surface. This well-fit pseudo-second-order model implies that the rate limiting step is correlated with the chemical adsorption and electronic forces through the sharing or exchange of electrons between the M-BC and ionized CIP species.
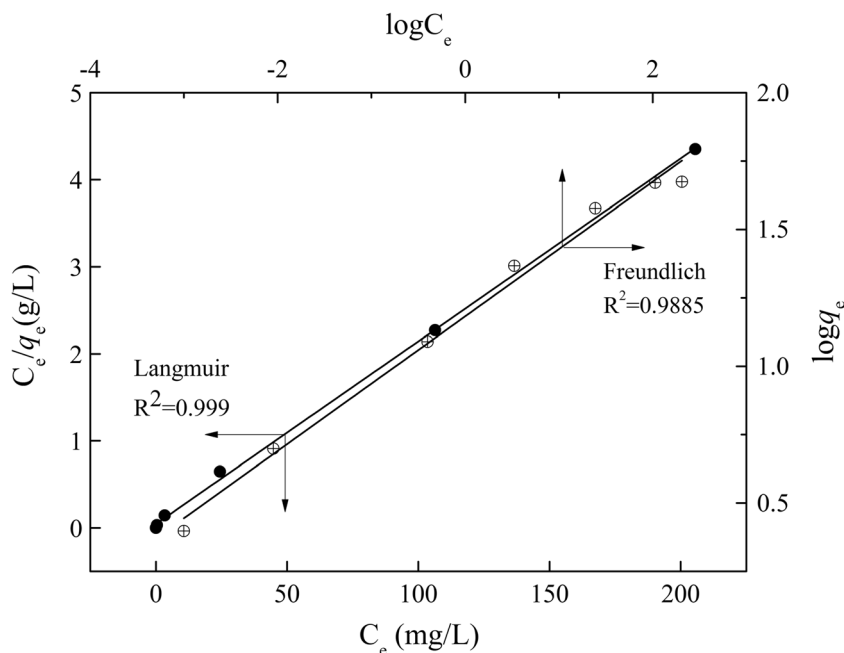
Adsorption isotherms

As shown in Fig. 7, the adsorption capacity of M-BC increased with increasing CIP concentration. To provide a better description of the adsorption mechanism, two typical adsorption models, the Langmuir (Eq. 3) and Freundlich (Eq. 4)

Table 2 Kinetic parameters of adsorption kinetics

C_0 (mg/L)	q_e (mg/g)	Pseudo-first-order kinetics			Pseudo-second-order kinetics		
		$q_{e,\ cal}$ (mg/g)	k_1 (min^{-1})	R^2	$q_{e,\ cal}$ (mg/g)	k_2 (g/mg min)	R^2
55	26.24	30.47	0.0079	0.639	26.25	0.0106	0.999
110	44.17	255.9	0.009	0.799	44.44	0.0040	0.999
220	60.37	1052.2	0.0057	0.701	60.61	0.0013	0.999

Fig. 7 Adsorption isotherms for CIP on M-BC

isotherm models, were applied to simulate the adsorption isotherms of CIP onto the M-BC.

$$\frac{C_e}{q_e} = \frac{C_e}{q_m} + \frac{1}{q_m K_L} \qquad (3)$$

$$\log q_e = \log K_f + \frac{1}{n} \log C_e \qquad (4)$$

C_e is the equilibrium concentration after adsorption (mg/L), q_e is the amount of CIP adsorbed per gram of AMBC (mg/g), K_L (L/mg) is the Langmuir constant, q_m (mg/g) is the maximum adsorption capacity of the isotherm model, K_f is the constant indicative of the relative adsorption capacity of MBC (mg/g) and $1/n$ is a constant.

According to the fitting parameters listed in Table 3, the R^2 values of the Langmuir and Freundlich isotherms were 0.9999 and 0.9885, respectively. The experiment data demonstrated that the Langmuir model fit the isotherms better than the Freundlich model. This is in agreement with other relevant study on oxytetracycline adsorption with maize straw biochar pyrolyzed at 600 °C (Jia et al. 2016). The Langmuir model is based on the assumption that the sorption occur at specific

sites on the surface of M-BC and is typically used to estimate whether the sorption process was favorable or unfavorable according to the constant separation factor (R_L) defined by McKay (McKay 1982).

$$R_L = \frac{1}{1 + K_L C_0} \qquad (6)$$

where C_0 is the highest initial CIP concentration (mg/L). The value of R_L indicates whether the shape of the isotherm is irreversible ($R_L = 0$), favorable ($0 < R_L < 1$), linear ($R_L = 1$) or unfavorable ($R_L > 1$). In the present study, the R_L value was 0.0072, indicating that the adsorption was favorable. The value of n in the Freundlich model was 4.065, suggesting that the adsorption condition was beneficial (a value of $n > 1$ represents a beneficial adsorption condition).

Effect of pH

The initial pH level that influences the surface charge of M-BC and the CIP species is an important factor for adsorption. Batch experiments with an initial pH ranging from 3 to 10, a CIP concentration of 200 mg/L and 0.05 g of M-BC were conducted for 12 h to study the optimum pH conditions for CIP adsorbed onto M-BC.

As shown in Fig. 8, the results demonstrated that the solution pH had significant effects on the efficiency of ciprofloxacin removal. The adsorption capacity increased with increasing pH from 3.0 to 6.0 and then greatly decreased with an increase in pH from 6.0 to 10.0. When the solution pH was approximately 6, the efficiency of ciprofloxacin removal

Table 3 Isotherm model parameters for the adsorption of CIP by BC

Freundlich		Langmuir	
K_f	15.223	q_m (mg/g)	47.62
n	4.065	K_L (L/mg)	0.4605
R^2	0.9885	R^2	0.9999

Fig. 8 Effect of the initial solution pH level on CIP removal
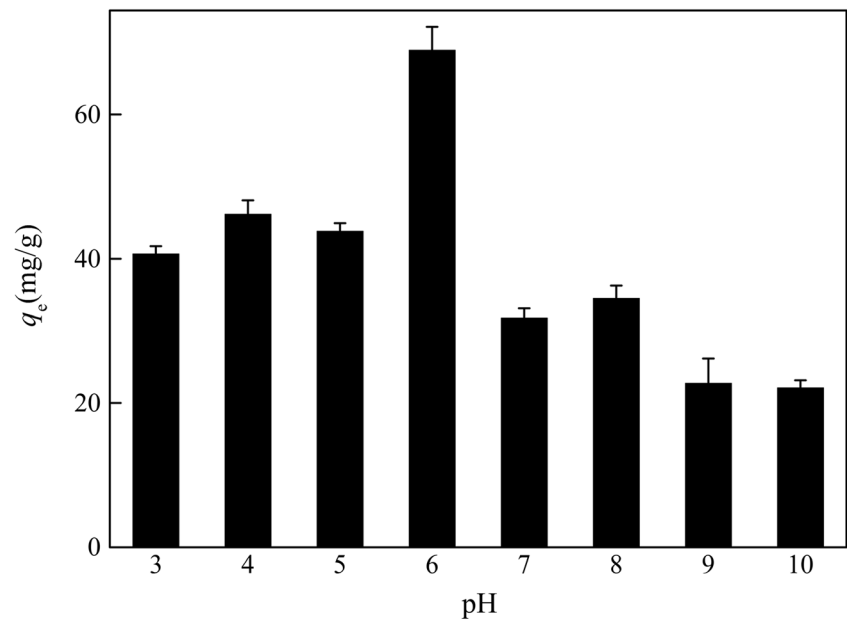
reached a maximum value of 68.9 ± 3.23 mg/g; this result indicates that if M-BC is used to remove wastewater containing ciprofloxacin, the removal efficiency can be increased by adjusting the pH of the wastewater to 6.

The surface charge of CIP is pH dependent, according to Vasudevan et al. (2009), CIP contains amino and carboxyl (pKa$_1$ = 6.18 and pKa$_2$ = 8.76). When pH < 6.18, cationic form was dominant and the biochar surface was typically negatively charged (Ahmad et al. 2014), which could facilitate the electrostatic attraction of cationic form, resulting in higher sorption. In the pH range from 6.18 to 8.76, zwitterionic form (CIPH$_2^+$) was dominant and the electrostatic interaction may be not responsible for the CIP sorption. At pH > 8.76, anionic form was dominant, and the q$_e$ values greatly declined because of the electrostatic repulsion between CIP$^-$ and negatively charged M-BC. Similar results were obtained for removal of ciprofloxacin from aqueous with natural clay montmorillonite by Jalil et al. (2015).

Conclusions

M-BC was successfully prepared by combining Fe^{2+}/ Fe^{3+} solution and biochar in alkaline conditions; they were analyzed using BET surface area, VSM, SEM-EDS, XRD, and FTIR techniques. M-BC was effective for CIP removal from the aqueous solution and can be separated with a magnet. The overall sorption of CIP on M-BC was both concentration and pH dependent, with a maximum adsorption capacity of approximately 68.9 ± 3.23 mg/g at pH 6.0. The adsorption of CIP by M-BC was found to follow the pseudo-second-order model, and it was better described by the Langmuir isotherm.

The results presented in this study indicate that the M-BC presents great potential as a low-cost, readily available, and recyclable adsorbent for the removal of CIP in wastewater treatments.

References

Ahmad M, Lee SS, Dou X, Mohan D, Sung JK, Yang JE, Ok YS (2012) Effects of pyrolysis temperature on soybean stover- and peanut shell-derived biochar properties and TCE adsorption in water. Bioresour Technol 118:536–544

Ahmad M, Rajapaksha AU, Lim JE, Zhang M, Bolan N, Mohan D, Vithanage M, Lee SS, Ok YS (2014) Biochar as a sorbent for contaminant management in soil and water: a review. Chemosphere 99: 19–33

Al-Wabel MI, Usman AR, El-Naggar AH, Aly AA, Ibrahim HM, Elmaghraby S, Al-Omran A (2015) Conocarpus biochar as a soil amendment for reducing heavy metal availability and uptake by maize plants. Saudi J Biol Sci 22:503–511

Ambashta RD, Sillanpää M (2010) Water purification using magnetic assistance: a review. J Hazard Mater 180:38–49

Berendonk TU, Manaia CM, Merlin C, Fatta-Kassinos D, Cytryn E, Walsh F, Bürgmann H, Sørum H, Norström M, Pons M-N (2015) Tackling antibiotic resistance: the environmental framework. Nat Rev Microbiol 13:310–317

Cheng XQ, Zhang C, Wang ZX, Shao L (2016) Tailoring nanofiltration membrane performance for highly-efficient antibiotics removal by mussel-inspired modification. J Membr Sci 499:326–334

Do MH, Phan NH, Nguyen TD, Pham TTS, Nguyen VK, Vu TTT, Nguyen TKP (2011) Activated carbon/Fe3O4 nanoparticle composite: fabrication, methyl orange removal and regeneration by hydrogen peroxide. Chemosphere 85:1269–1276

Fan T, Pan DK, Zhang H (2011) Study on formation mechanism by monitoring the morphology and structure evolution of nearly monodispersed Fe3O4 submicroparticles with controlled particle sizes. Ind Eng Chem Res 50:9009–9018

García-Galán MJ, Díaz-Cruz MS, Barceló D (2011) Occurrence of sulfonamide residues along the Ebro river basin: removal in wastewater treatment plants and environmental impact assessment. Environ Int 37:462–473

Inyang M, Dickenson E (2015) The potential role of biochar in the removal of organic and microbial contaminants from potable and reuse water: a review. Chemosphere 134:232–240

Jalil MER, Baschini M, Sapag K (2015) Influence of pH and antibiotic solubility on the removal of ciprofloxacin from aqueous media using montmorillonite. Appl Clay Sci 114:69–76

Ji Y, Fan Y, Liu K, Kong D, Lu J (2015) Thermo activated persulfate oxidation of antibiotic sulfamethoxazole and structurally related compounds. Water Res 87:1–9

Jia MY, Wang F, Jin X, Song Y, Bian YR, Boughner LA, Yang XL, Gu CG, Jiang X, Zhao QG (2016) Metal ion-oxytetracycline interactions on maize straw biochar pyrolyzed at different temperatures. Chem Eng J 304:934–940

Li HB, Zhang D, Han XZ, Xing BS (2014) Adsorption of antibiotic ciprofloxacin on carbon nanotubes: pH dependence and thermodynamics. Chemosphere 95:150–155

Li WY, Loyola-Licea C, Crowley DE, Ahmad Z (2016) Performance of a two-phase biotrickling filter packed with biochar chips for treatment of wastewater containing high nitrogen and phosphorus concentrations. Process Saf Environ Prot 102:150–158

Lian F, Sun BB, Song ZG, Zhu LY, Qi XH, Xing BS (2014) Physicochemical properties of herb-residue biochar and its sorption to ionizable antibiotic sulfamethoxazole. Chem Eng J 248:128–134

Lim SF, Zheng YM, Chen JP (2009) Organic arsenic adsorption onto a magnetic sorbent. Langmuir 25:4973–4978

Lonappan L, Rouissi T, Das RK, Brar SK, Ramirez AA, Verma M, Surampalli RY, Valero JR (2016) Adsorption of methylene blue on biochar microparticles derived from different waste materials. Waste Manag 49:537–544

Martins AC, Pezoti O, Cazetta AL, Bedin KC, Yamazaki DA, Bandoch GF, Asefa T, Visentainer JV, Almeida VC (2015) Removal of tetracycline by NaOH-activated carbon produced from macadamia nut shells: kinetic and equilibrium studies. Chem Eng J 260:291–299

McKay G (1982) Adsorption of dyestuffs from aqueous solutions with activated carbon I: equilibrium and batch contact-time studies. J Chem Technol Biotechnol 32:759–772

Meira SMM, Jardim AI, Brandelli A (2015) Adsorption of nisin and pediocin on nanoclays. Food Chem 188:161–169

Mohan D, Kumar H, Sarswat A, Alexandre-Franco M, Pittman CU (2014) Cadmium and lead remediation using magnetic oak wood and oak bark fast pyrolysis bio-chars. Chem Eng J 236:513–528

Mohan D, Singh P, Sarswat A, Steele PH, Pittman CU (2015) Lead sorptive removal using magnetic and nonmagnetic fast pyrolysis energy cane biochars. J Colloid Interface Sci 448:238–250

Nodeh HR, Ibrahim WAW, Ali I, Sanagi MM (2016) Development of magnetic graphene oxide adsorbent for the removal and preconcentration of As (III) and As (V) species from environmental water samples. Environ Sci Pollut R: 1–15

Shan DN, Deng SB, Zhao TN, Wang B, Wang YJ, Huang J, Yu G, Winglee J, Wiesner MR (2016) Preparation of ultrafine magnetic biochar and activated carbon for pharmaceutical adsorption and subsequent degradation by ball milling. J Hazard Mater 305:156–163

Sharma VK, Johnson N, Cizmas L, McDonald TJ, Kim H (2016) A review of the influence of treatment strategies on antibiotic resistant bacteria and antibiotic resistance genes. Chemosphere 150:702–714

Sun L, Wan SG, Luo WS (2013) Biochars prepared from anaerobic digestion residue, palm bark, and eucalyptus for adsorption of cationic methylene blue dye: characterization, equilibrium, and kinetic studies. Bioresour Technol 140:406–413

Tian XK, Wang WK, Tian N, Zhou CX, Yang C, Komarneni S (2016) Cr (VI) reduction and immobilization by novel carbonaceous modified magnetic Fe3O4/halloysite nanohybrid. J Hazard Mater 309:151–156

Tytłak A, Oleszczuk P, Dobrowolski R (2015) Sorption and desorption of Cr (VI) ions from water by biochars in different environmental conditions. Environ Sci Pollut R 22:5985–5994

Vasudevan D, Bruland GL, Torrance BS, Upchurch VG, MacKay AA (2009) pH-dependent ciprofloxacin sorption to soils: interaction mechanisms and soil factors influencing sorption. Geoderma 151:68–76

Wang SY, Tang YK, Li K, Mo YY, Li HF, Gu ZQ (2014) Combined performance of biochar sorption and magnetic separation processes for treatment of chromium-contained electroplating wastewater. Bioresour Technol 174:67–73

Wu WD, Li JH, Niazi NK, Müller K, Chu YC, Zhang LL, Yuan GD, Lu KP, Song ZL, Wang HL (2016) Influence of pyrolysis temperature on lead immobilization by chemically modified coconut fiber-derived biochars in aqueous environments. Environ Sci Pollut R 23:22890–22896

Xu XY, Cao XD, Zhao L, Wang HL, Yu HR, Gao B (2013) Removal of Cu, Zn, and Cd from aqueous solutions by the dairy manure-derived biochar. Environ Sci Pollut R 20:358–368

Yang K, Yang JJ, Jiang Y, Wu WH, Lin DH (2016) Correlations and adsorption mechanisms of aromatic compounds on a high heat temperature treated bamboo biochar. Environ Pollut 210:57–64

Zhang M, Gao B, Varnoosfaderani S, Hebard A, Yao Y, Inyang M (2013) Preparation and characterization of a novel magnetic biochar for arsenic removal. Bioresour Technol 130:457–462

Zhang QQ, Ying GG, Pan CG, Liu YS, Zhao JL (2015) Comprehensive evaluation of antibiotics emission and fate in the river basins of China: source analysis, multimedia modeling, and linkage to bacterial resistance. Environ Sci Technol 49:6772–6782

Zhou LC, Ji LQ, Ma PC, Shao YM, Zhang H, Gao WJ, Li YF (2014a) Development of carbon nanotubes/CoFe2O4 magnetic hybrid material for removal of tetrabromobisphenol A and Pb (II). J Hazard Mater 265:104–114

Zhou YM, Gao B, Zimmerman AR, Chen H, Zhang M, Cao XD (2014b) Biochar-supported zerovalent iron for removal of various contaminants from aqueous solutions. Bioresour Technol 152:538–542

Zhu XD, Liu YC, Zhou C, Zhang SC, Chen JM (2014) Novel and high-performance magnetic carbon composite prepared from waste hydrochar for dye removal. ACS Sustain Chem Eng 2:969–977